symmetry

MDPI

Article

A Self-Similar Approach to Study Nanofluid Flow Driven by a Stretching Curved Sheet

Kashif Ali [1], Wasim Jamshed [2,*], Sohail Ahmad [1,3], Hina Bashir [3], Shahzad Ahmad [3] and El Sayed M. Tag El Din [4]

[1] Department of Basic Sciences and Humanities, Muhammad Nawaz Sharif University of Engineering and Technology, Multan 60000, Pakistan
[2] Department of Mathematics, Capital University of Science and Technology (CUST), Islamabad 44000, Pakistan
[3] Centre for Advanced Studies in Pure and Applied Mathematics, Bahauddin Zakariya University, Multan 60800, Pakistan
[4] Electrical Engineering, Faculty of Engineering and Technology, Future University in Egypt, New Cairo 11835, Egypt
* Correspondence: wasiktk@hotmail.com

Abstract: Nano-fluids have considerable importance in the field of thermal development that relates to several industrial systems. There are some key applications in recent construction systems flow, as well as microscale cooling gadgets and microstructure electric gadgets for thermal migration. The current investigation concludes the study of electrically conducting nano-fluid flow and heat transfer analysis in two-dimensional boundary layer flow over a curved extending surface in the coexisting of magnetic field, heat generation and thermal radiation. The small sized particles of copper (Cu) are taken as nanoparticles and water is assumed to be the base fluid. We used quasi-linearization and central difference approximation to numerically solve the system of coupled equations obtained from the partial differential equations (PDEs) by incorporating the concept of similarity. The impacts of non-dimensional parameters on velocity, concentration and thermal profiles have been discussed with the help of suitable graphs and tables. It has been noticed that the velocity decelerated with the effect of the magnetic field interaction parameter. Thermal radiation caused an increase in temperature.

Keywords: nanofluid; magnetic field; curved stretching sheet; thermal radiation; quasi linearization technique

Citation: Ali, K.; Jamshed, W.; Ahmad, S.; Bashir, H.; Ahmad, S.; Tag El Din, E.S.M. A Self-Similar Approach to Study Nanofluid Flow Driven by a Stretching Curved Sheet. *Symmetry* **2022**, *14*, 1991. https://doi.org/10.3390/sym14101991

Academic Editors: Ghulam Rasool and Raffaele Barretta

Received: 6 August 2022
Accepted: 17 September 2022
Published: 23 September 2022

1. Introduction

Many researchers have been interested in heat transportation and flow analysis of a curved stretching surface in the past few decades due to its extensive range of applications in the fields of engineering and industry. Some of the applications are extrusion of rubber, drawing plastic films, metal spinning, filaments, glass blowing, paper production and crystal growing. In all the above-mentioned processes, the final worth of the products depends not only on the heat transportation rate but also on skin friction at the surface. Naveed et al. [1] numerically examined the MHD electrically conducting boundary layer flow of micro-structured fluid over a curved surface. Moreover, a curvilinear coordinate system has been adopted in order to formulate the mathematical model. Misra et al. [2] described incompressible visco-elastic electrically conducting fluid flow with allowance for external magnetic field and transfer of heat in a parallel plate channel having extending walls. It has also been revealed that due to stretching walls, back flow occurs near the mid of the channel. Abbas et al. [3] analyzed viscous fluid flow and heat transmission with the effect of a constant magnetic field over a curved stretching sheet. A curvilinear coordinate system has also been used to govern flow equations. Abbas et al. [4] investigated two-dimensional visco-elastic electrically conducting boundary layer fluid flow with the effect of heat generation over shrinking/extending surface. Hayat et al. [5] discussed

two-dimensional steady micropolar flow over a non-linear expanding surface, while mass and heat transport with the effects of thermal radiation on micropolar unsteady fluid have been studied by applying the homotopy analysis method in [6].

Kanti et al. [7] presented an experimental investigation to examine the effect of uniform heat flux on nanofluid flow through a copper tube. The thermal characteristics of fly ash nanofluid were examined by Kanti et al. [8]. They suggested that employing water-based fly ash nanoparticles can help diminish ecological pollution. Further, they apply fly ash nanomolecules for heat transfer performance, which is more useful. A three-dimensional wavy microchannel turbulent flow was analyzed by Bazdar et al. [9]. They noticed variations in flow and heat transfer characteristics with changes in the CuO nanoparticle concentration and wavelength of the sinusoidal microchannel. Sarlak et al. [10] numerically investigated water-based aluminum oxide nanofluid flow in a closed enclosure, taking into account the effect of a homogeneous magnetic field. Ishak et al. [11] examined the stretching permeable surface of a laminar unsteady boundary layer flow and this unsteadiness in temperature and flow fields became the reason for time dependence on surface temperature and stretching velocity. Javad et al. [12] described the flow of micropolar boundary layer fluid over a stretched surface in a rotating frame of reference. Rasool et al. [13,14] numerically investigated the flow of Multi-Walled Carbon Nanoparticles and Maxwell nanofluids subject to entropy generation and Lorentz force.

Kumar [15] used the finite element method to discuss mass and heat transport analysis in hydro-magnetic flow over a curved sheet. Mahmood et al. [16] investigated the effects of slip parameter and heat transferal analysis for electrically conducting flow of micro-structured fluid over a curved expanding sheet with coexistence of heat generation as well as transverse magnetic field. Makinde [17] defined geophysical applications in thermal insulation, geothermal tanks, and improvement in oil recovery and cooling of nuclear reactors. Nazar et al. [18] elaborated steady two-dimensional micropolar fluid flow at the point of stagnation over a stretched sheet using the Keller-box method. Sajid et al. [19,20] used the Runge-Kutta method to discuss dimensionless curvature, which causes an increase in boundary layer flow. Furthermore, they used the same numerical method to find the results of micro constituents' flow over a curved sheet with the flow at the point of stagnation in the presence of a magnetic field and the flow over a vertical semi-infinite permeable sheet, respectively. Raju et al. [21] and Reddy [22] analyzed the mass and heat transferal characteristics of Casson fluid, taking into account the effect of thermal radiation. An exponentially extending permeable surface was used as the geometry. Ibrahim et al. [23] discussed mixed convection MHD Casson fluid flow over a non-linearly permeable extending sheet with heat sink/source, viscous dissipation, thermal radiation, suction and chemical reaction. Ghadikolaei et al. [24] studied the heat transport and micropolar boundary layer flow of incompressible TiO_2 water with nano-particles in the presence of thermal radiation. Khan et al. [25] described heterogeneous-homogenous reactions with characteristics of heat transfer and electrically conducting boundary layer fluid flow over stretched sheets. Nasir et al. [26] discussed the computations and modeling of rotating three-dimensional MHD nano-fluid flow through an extending surface.

Khan et al. [27] analyzed the properties of heat transport and steady flow in a permeable media about thin-film second-grade fluid over a stretching sheet. Khan et al. [28] investigated the flow with the influence of multiple slips on an axi-symmetric buoyant MHD nano-fluid over an expanding sheet. Mabood et al. [29] described the incompressible flow of a Jeffery fluid at the point of stagnation over a stretched sheet. Akbar et al. [30] presented a numerical analysis of viscous unsteady MHD nano-fluid flow of metallic nanoparticles in a channel with walls and a porous medium. Two cases of thermal conductivity are studied in heat and mass transfer analysis through the H-C model. Hady et al. [31] discussed nano-fluid flow in a permeable sheet of stream wise distance x with the influence of thermophoresis as well as Brownian motion. Ahmad et al. [32] numerically investigated MHD two-dimensional nano-fluid flow over cone/plate with the help of finite difference discretization. Iqbal et al. [33] studied two orthogonally moving coaxial disks of hydro-

magnetic unsteady viscous incompressible water-based nano-fluid flow with the effects of suction. Further recent investigations relevant to the concerned topic can be seen in refs. [34–43].

According to the author's best information, no endeavor is available in the literature that deals with electrically conducting nano-fluid flow along a curved extending surface, taking into consideration the simultaneous effects of external magnetic field, heat generation and thermal radiation. The current investigation is an attempt in this direction. In the present work, a numerical model is developed in order to solve the governing equations by incorporating the quasi-linearization technique. The results are scrutinized through graphs and tables. Moreover, the present investigation provides a basis for many science and engineering applications.

2. Mathematical Formulation

The assumptions for the flow model incorporate the magnetic field of strength B_o, stretching sheet, and incompressible fluid. The flow geometry is presented in Figure 1.

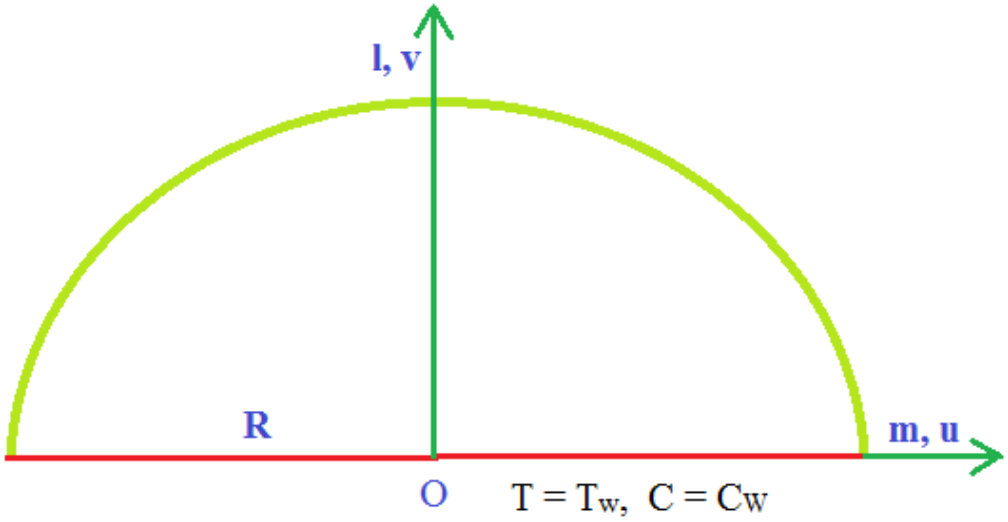

Figure 1. Geometry of the problem.

A very small magnetic Reynolds number is assumed for the magnetic field of strength B_o. The origin is fixed, which is represented by O and two reverse, but equal forces are utilized along m and l directions. The temperatures at the boundary of the sheet and far away from the sheet are, respectively, represented by T_w and T_∞. These temperatures are taken in such a way that the temperature T_w at the boundary of the sheet is greater than that the ambient temperature T_∞. The difference between both these temperatures can be given as $\Delta T = T_w - T_\infty$. Moreover, l direction is normal to the origin. The curved sheet takes the velocity $u = am$.

Incorporating the aforementioned assumptions, we write the leading equations as [1]:

$$\frac{\partial}{\partial l}\{(l+R)v\} + R\frac{\partial u}{\partial m} = 0, \tag{1}$$

$$\frac{u^2}{R+l} = \frac{1}{\rho_{nf}}\frac{\partial p}{\partial l}, \tag{2}$$

$$v\frac{\partial u}{\partial l} + \frac{Ru}{R+l}\frac{\partial u}{\partial m} + \frac{uv}{R+l} = -\frac{1}{\rho_{nf}}\frac{R}{R+l}\frac{\partial p}{\partial m} + \nu_{nf}\left(\frac{\partial^2 u}{\partial l^2} + \frac{1}{R+l}\frac{\partial u}{\partial l} - \frac{u}{(R+l)^2}\right) - \frac{\sigma B_o^2}{\rho_{nf}}u, \tag{3}$$

$$(\rho c_p)_{nf}\left[v\frac{\partial T}{\partial l} + \frac{uR}{R+l}\frac{\partial T}{\partial m}\right] = k_{nf}\left[\frac{\partial^2 T}{\partial l^2} + \frac{1}{R+l}\frac{\partial T}{\partial l}\right] + \frac{1}{R+l}\frac{\partial}{\partial l}(R+l)q_r + Q(T-T_\infty), \tag{4}$$

$$v\frac{\partial C}{\partial l} + \frac{Ru}{R+l}\frac{\partial C}{\partial m} = D\nabla^2 C - k_1^*(C - C_\infty). \tag{5}$$

Here, the components of velocity in m and l directions are u, v respectively with pressure p and density of the nano-fluid is taken to be ρ_{nf}. Additionally, μ_{nf}, v_{nf} are viscosity and kinematics viscosity of the nano-fluid flow while c_p, C and C_∞ are shown as specific heat at constant pressure, concentration and concentration of the ambient fluid, respectively. Thermal conductivity is ${k_1}^*$, q_r is radioactive heat flux and Q represented volumetric rate of the heat source. It is worth mentioning here that the pressure is no longer constant for a curved stretching sheet inside the boundary layer flow.

The boundary conditions are given by:

$$\left.\begin{array}{l} u = am + L\left(\frac{\partial u}{\partial l} - \frac{u}{R+l}\right), \quad v = 0, \quad T = T_w, \quad C = C_w \text{ at } l = 0, \\ u \to 0, \quad \frac{\partial u}{\partial l} \to 0, \quad T \to T_\infty, \quad C = C_\infty \text{ as } r \to \infty. \end{array}\right\} \tag{6}$$

Here μ_{nf} represents the dynamic viscosity, L is the slip parameter, ρ_{nf} density, α_{nf} thermal diffusivity and $(\rho c_p)_{nf}$ heat capacitance of nano-fluid flow respectively, given as

$$\mu_{nf} = \mu_f(1-\varphi)^{-2.5}, \tag{7}$$

$$\rho_{nf} = \phi\rho_s + (1-\phi)\rho_f, \tag{8}$$

$$\alpha_{nf} = \frac{k_{nf}}{(\rho c_p)_{nf}}, \tag{9}$$

$$(\rho c_p)_{nf} = \phi(\rho c_p) + (1-\phi)(\rho c_p)_f. \tag{10}$$

Here, the volume fraction of the solid nanoparticles is represented by ϕ. Restricted to nanoparticles, the thermal conductivity of nanofluid is approximated as

$$\frac{k_{nf}}{k_f} = \left[\frac{k_s + 2k_f - 2\phi\left(k_f - k_s\right)}{k_s + 2k_f - 2\phi\left(k_f - k_s\right)}\right]. \tag{11}$$

In Equations (6)–(10), the subscripts, such as f denotes the base fluid, nf is used for nanofluid and s for nano-solid particles, respectively. The thermal attributes of nanoparticles, as well as base fluid, are portrayed in Table 1.

Table 1. Thermal characteristics of water and copper particles.

	c_p (J/kgK)	ρ (kg/m^3)	k (W/mK)	$\beta \times 10^5$ (K^{-1})
Pure water	4179	997.1	0.613	21
Cu	385	89.33	401	1.67

We incorporate Rosseland approximation to calculate the relation for thermal radiation:

$$q_r = -\frac{4\sigma^*}{3k^*}\left(\frac{\partial T^4}{\partial r}\right), \tag{12}$$

where σ^* denotes the Stefan–Boltzmann constant while the mean absorption coefficient is k^*. By using the assumption, the temperature diffusion in flow is sufficiently small so that the Taylor series can be used to expand term T^4. Omitting the higher order terms, we have:

$$T^4 \equiv 4TT^3{}_\infty - 3T^4{}_\infty. \tag{13}$$

In view of Equations (6) and (7), Equation (4) can be written as:

$$v\frac{\partial T}{\partial l}+\frac{uR}{R+l}\frac{\partial T}{\partial m}=\frac{k_{nf}}{(\rho c_p)_{nf}}\left(1+\frac{16\sigma^* T^3_\infty}{3k_f k^*}\frac{k_f}{k_{nf}}\right)\left[\frac{\partial^2 T}{\partial l^2}+\frac{1}{R+l}\frac{\partial T}{\partial l}\right]+\frac{Q}{(\rho c_p)_{nf}}(T-T_\infty), \tag{14}$$

We obtained the radiation parameter as $Rd=\frac{16\sigma^* T^3_\infty}{3k_f k^*}$, so Equation (13) becomes

$$v\frac{\partial T}{\partial l}+\frac{uR}{R+l}\frac{\partial T}{\partial m}=\frac{1}{\Pr}\frac{k_{nf}}{k_f}\left(1+Rd\frac{k_f}{k_{nf}}\right)\left[\frac{\partial^2 T}{\partial l^2}+\frac{1}{R+l}\frac{\partial T}{\partial l}\right]+\frac{Q}{(\rho c_p)_{nf}}(T-T_\infty), \tag{15}$$

We will use the following conversion to reduce the aforementioned equation, such that

$$\left.\begin{array}{l} u=amf'(\eta), v=\frac{-R}{R+l}\sqrt{av_f}f(\eta), p=\rho a^2 m^2 P(\eta), \eta=\sqrt{\frac{a}{v_f}}l \\ T=T_\infty+(Am/\delta)\theta(\eta), \theta(\eta)=\frac{T-T_\infty}{T_w-T_\infty}, \chi(\eta)=\frac{C-C_\infty}{C_w-C_\infty}, \end{array}\right\}, \tag{16}$$

By applying (16), Equations (2)–(5) yield

$$\frac{\partial P}{\partial \eta}=\frac{f'^2}{k+\eta}, \tag{17}$$

$$P\frac{2k}{k+\eta}=\frac{v_{nf}}{v_f}\left\{f'''+\frac{f''}{k+\eta}-\frac{f'}{(k+\eta)^2}\right\}-\frac{k}{k+\eta}f'^2+\frac{k}{k+\eta}ff''+\frac{k}{(k+\eta)^2}ff'-Mf', \tag{18}$$

$$\left(1+Rd\frac{k_f}{k_{nf}}\right)\left(\theta''+\frac{1}{k+\eta}\theta'\right)-\Pr\frac{k_f}{k_{nf}}\left[\phi_3\frac{k}{k+\eta}\left(f'\theta-f\theta'\right)\right]+\frac{k_f}{k_{nf}}\Pr\lambda_1\theta=0 \tag{19}$$

$$\chi''+\left(\frac{1}{k+\eta}+\frac{k}{k+\eta}f\,S_c\right)\chi'-\gamma S_c\chi=0, \tag{20}$$

The parallel boundary conditions become:

$$\left.\begin{array}{l} |f(0)=1, f'(0)=1+\kappa\left[f''(0)-\frac{f'(0)}{k}\right], \theta(0)=1, \chi(0)=1, \\ |f'(\infty)=0, f''(\,\infty)=0, \theta(\infty)=0, \chi(\infty)=0. \end{array}\right\}. \tag{21}$$

By using Equations (17) and (18), the pressure term can be eliminated as

$$\begin{array}{l} f^{iv}+\frac{2}{k+\eta}f'''-\frac{1}{(k+\eta)^2}f''+\frac{1}{(k+\eta)^3}f'+\phi_1\left[-\frac{k}{(k+\eta)}(f'f''-ff''')-\frac{k}{(k+\eta)^2}\left(f'^2-ff''\right)\right. \\ \left.-\frac{k}{(k+\eta)^3}ff'-\frac{M}{\phi_2}\left(f''+\frac{f'}{k+\eta}\right)\right]=0, \end{array} \tag{22}$$

when we obtained $f(\eta)$ as fluid velocity, one can determine pressure from Equation (18).

$$P=\frac{k+\eta}{2k}\left(\frac{1}{\phi_1}\left(f'''+\frac{f''}{k+\eta}-\frac{f'}{(k+\eta)^2}\right)-\frac{k}{k+\eta}f'^2+\frac{k}{k+\eta}ff''+\frac{1}{(k+\eta)^2}ff'-Mf'\right) \tag{23}$$

where

$$\phi_1=(1-\phi)^{2.5}\left[1-\phi+\phi\left(\frac{\rho_s}{\rho_f}\right)\right],\ \phi_2=1-\phi+\phi\left(\frac{\rho_s}{\rho_f}\right),\ \phi_3=1-\phi+\phi\frac{(\rho c_p)_s}{(\rho c_p)_f},\ \phi_4=(1-\phi)^{2.5}\left[1-\phi+\phi\frac{(\rho c_p)_s}{(\rho c_p)_f}\right]. \tag{24}$$

Dimensionless radius of curvature, Prandtl number, Magnetic parameter, heat generation parameter, Schmidt number, slip parameters and chemical reaction are:

$$k=R\sqrt{\frac{a}{v_f}},\ P_r=\frac{\mu_f(c_p)_f}{\kappa_f},\ M=\frac{\sigma B_0^2}{\rho_f a},\ \lambda_1=\frac{Q}{a(\rho c_p)_f},\ \gamma=\frac{k_1^*}{a},\ \kappa=\frac{L}{\sqrt{a/v}},\ Sc=\frac{v_f}{D}. \tag{25}$$

The surface drag coefficient, Nusselt and Sherwood number are taken in the direction of m, such that

$$C_f = \tau_{lm}/\rho_f u_w^2,\ Nu_m = mq_w/k_f(T_w - T_\infty),\ Sh = mj_w/D(C_w - C_\infty)$$

Here τ_{lm} represented as wall shear stress while q_w and j_w are heat and mass fluxes at the wall in the direction of m, defined as

$$\tau_{lm} = -\left(\mu_{nf}\right)\left(\frac{\partial u}{\partial l} - \frac{u}{l+R}\right)\Big|_{l=0},\quad q_w = -k_{nf}\left(1 + \frac{16\sigma^* T_\infty^3}{3k_f k^*}\frac{k_f}{k_{nf}}\right)\frac{\partial T}{\partial l}\Big|_{l=0}, j_w = -D\,\frac{\partial C}{\partial l}\Big|_{l=0}$$

$$C_f = -(\mathrm{Re}_m)^{1/2}(1-\phi)^{-2.5}\left(f''(0) - \frac{f'(0)}{k}\right),\ Nu_m = -(\mathrm{Re}_m)^{1/2}\frac{k_{nf}}{k_f}\left(1 + Rd\frac{k_f}{k_{nf}}\right)\theta'(0),\ Sh = -(\mathrm{Re}_m)^{1/2}\phi'(0)$$

where the local Reynolds number is defined as $\mathrm{Re}_m = am^2/v_f$.

3. Computational Procedure

This section describes numerical aspects of the technique of quasi-linearization, which is basically a generalization of the Newton–Raphson method for functional equations. It provides a sequence of functions and linearizes a nonlinear equation that converges quickly to the solution of the original non-linear equation. A quasi-linearization technique is used to overcome certain numerical difficulties in non-linear initial value problems and is much more efficient for non-linear boundary value problems. In the present study, we discuss the quasi-linearization of non-linear ordinary differential equations.

3.1. Quasi-Linearization Method

Now applying quasi-linearization with the solutions for sequences of vectors, which are f^k, θ^k, χ^k on Equation (22) such that (putting $f = \Upsilon$):

$$G\left(\Upsilon^{(k)}, \Upsilon'^{(k)}, \Upsilon''^{(k)}, \Upsilon'''^{(k)}, \Upsilon^{iv(k)}\right) = \Upsilon^{iv} + \tfrac{2}{k+\eta}\Upsilon''' - \tfrac{1}{(k+\eta)^2}\Upsilon'' + \tfrac{1}{(k+\eta)^3}\Upsilon' + \phi_1\Big[-\tfrac{k}{(k+\eta)}(\Upsilon'\Upsilon'' - \Upsilon\Upsilon''') - \tfrac{k}{(k+\eta)^2}\left(\Upsilon'^2 - \Upsilon\Upsilon''\right) - \tfrac{k}{(k+\eta)^3}\Upsilon\Upsilon' - \tfrac{M}{\phi_2}\left(\Upsilon'' + \tfrac{\Upsilon'}{k+\eta}\right)\Big], \tag{26}$$

$$G\left(\Upsilon^{(k)}, \Upsilon'^{(k)}, \Upsilon''^{(k)}, \Upsilon'''^{(k)}, \Upsilon^{iv(k)}\right) + \left(\Upsilon^{(k+1)} - \Upsilon^{(k)}\right)\tfrac{\partial G}{\partial \Upsilon^{(k)}} + \left(\Upsilon'^{(k+1)} - \Upsilon'^{(k)}\right)\tfrac{\partial G}{\partial \Upsilon'^{(k)}} + \left(\Upsilon''^{(k+1)} - \Upsilon''^{(k)}\right)\tfrac{\partial G}{\partial \Upsilon''^{(k)}} + \left(\Upsilon'''^{(k+1)} - \Upsilon'''^{(k)}\right)\tfrac{\partial G}{\partial \Upsilon'''^{(k)}} + \left(\Upsilon^{iv(k+1)} - \Upsilon^{iv(k)}\right)\tfrac{\partial G}{\partial \Upsilon^{iv(k)}} = 0, \tag{27}$$

In the above equation, applying central difference approximation to the derivatives becomes

$$\begin{bmatrix} \Upsilon^{iv(k)} + \tfrac{2}{(k+\eta)}\Upsilon'''^{(k)} - \tfrac{1}{(k+\eta)^2}\Upsilon''^{(k)} + \tfrac{1}{(k+\eta)^3}\Upsilon'^{(k)} + \phi_1\Big[-\tfrac{k}{k+\eta}\left(\Upsilon'^{(k)}\Upsilon''^{(k)} - \Upsilon^{(k)}\Upsilon'''^{(k)}\right) - \tfrac{k}{(k+\eta)^2}\Big(\Upsilon'^{(k)}\Upsilon''^{(k)} \\ -\Upsilon^{(k)}\Upsilon'''^{(k)}\Big) - \tfrac{k}{(k+\eta)^3}\Upsilon^{(k)}\Upsilon'^{(k)} - \tfrac{M}{\phi_2}\left(\Upsilon'^{(k)} + \tfrac{\Upsilon'^{(k)}}{(k+\eta)}\right)\Big] + \phi_1\left[\tfrac{k}{(k+\eta)}\Upsilon'''^{(k)} + \tfrac{k}{(k+\eta)^2}\Upsilon''^{(k)} - \tfrac{k}{(k+\eta)^3}\Upsilon'^{(k)}\right]\Big(\Upsilon^{(k+1)} \\ -\Upsilon^{(k)}\Big) + \left[\tfrac{1}{(k+\eta)^2} - \phi_1\tfrac{k}{(k+\eta)}\Upsilon''^{(k)} - 2\phi_1\tfrac{k}{(k+\eta)^2}\Upsilon'^{(k)} - \phi_1\tfrac{k}{(k+\eta)^3}\Upsilon^{(k)} - \tfrac{M\phi_1}{\phi_2}\left(1 + \tfrac{1}{(k+\eta)}\right)\right]\left(\Upsilon'^{(k+1)} - \Upsilon'^{(k)}\right) \\ +\left[-\tfrac{1}{(k+\eta)^2} - \phi_1\tfrac{k}{(k+\eta)}\Upsilon'^{(k)} + \phi_1\tfrac{k}{(k+\eta)^2}\Upsilon^{(k)}\right]\left(\Upsilon''^{(k+1)} - \Upsilon''^{(k)}\right) + \left[\tfrac{2}{(k+\eta)} + \phi_1\tfrac{k}{(k+\eta)}\Upsilon^{(k)}\right]\left(\Upsilon'''^{(k+1)} - \Upsilon'''^{(k)}\right) \\ +\left(\Upsilon^{iv(k+1)} - \Upsilon^{iv(k)}\right) = 0, \end{bmatrix} \tag{28}$$

Simplified as

$$\left[\begin{array}{l}\phi_1\frac{k}{(k+\eta)^2}\Upsilon'^{2(k)}+\phi_1\frac{k}{(k+\eta)}\left(\Upsilon'''^{(k)}\Upsilon^{(k+1)}-\Upsilon'''^{(k)}\Upsilon^{(k)}\right)+\phi_1\frac{k}{(k+\eta)^2}\left(\Upsilon''^{(k)}\Upsilon^{(k+1)}-\Upsilon''^{(k)}\Upsilon^{(k)}\right)+\phi_1\frac{k}{(k+\eta)^3}\left(\Upsilon'^{(k)}\Upsilon^{(k)}\right.\\ \left.-\Upsilon'^{(k)}\Upsilon^{(k+1)}\right)+\phi_1\frac{k}{(k+\eta)}\left(\Upsilon'^{(k)}\Upsilon''^{(k)}-\Upsilon'^{(k)}\Upsilon''^{(k+1)}\right)+\frac{1}{(k+\eta)^3}\Upsilon'^{(k+1)}-\phi_1\frac{k}{(k+\eta)}\Upsilon''^{(k)}\Upsilon'^{(k+1)}-2\phi_1\frac{k}{(k+\eta)^2}\Upsilon'^{(k)}\Upsilon'^{(k+1)}\\ -\phi_1\frac{k}{(k+\eta)^3}\Upsilon^{(k)}\Upsilon'^{(k+1)}-\frac{M\phi_1}{\phi_2}\left(1+\frac{1}{(k+\eta)}\right)\Upsilon'^{(k+1)}-\frac{1}{(k+\eta)^2}\Upsilon''^{(k+1)}+\phi_1\frac{k}{(k+\eta)^2}\Upsilon^{(k)}\Upsilon''^{(k+1)}+\frac{2}{(k+\eta)^2}\Upsilon'''^{(k+1)}\\ +\phi_1\frac{k}{(k+\eta)}\Upsilon^{(k)}\Upsilon'''^{(k+1)}+\Upsilon^{iv(k+1)}=0,\end{array}\right] \quad (29)$$

Procedure Steps

(1) $f^{(0)}, \theta^{(0)}$ and $\chi^{(0)}$ are the initial guesses to assure the boundary conditions, which are specified in equation.
(2) Set $f^{(1)}$ in Equation (28) to present the solution of the linear system.
(3) We are solving a linear system by means of $f^{(1)}$ forgetting $\theta^{(1)}$ and $\chi^{(1)}$.
(4) By using new initial guesses that are $f^{(1)}, \theta^{(1)}$ and $\chi^{(1)}$ which converges to f, θ and χ, repeating this process to create sequences $f^{(k)}, \theta^{(k)}$ and $\chi^{(k)}$.
(5) We are creating four sequences until

$$\max\left\{\left|\left|f^{(k+1)}-f^{(k)}\right|\right|_{L_\infty}, \left|\left|\theta^{(k+1)}-\theta^{(k)}\right|\right|_{L_\infty}, \left|\left|\chi^{(k+1)}-\chi^{(k)}\right|\right|_{L_\infty}\right\} < 10^{-6}$$

By applying the extrapolation polynomial, one can expand the solution with an order of accuracy.

4. Results and Discussion

The results and discussion both in tabular and graphical form are presented with their interpretations for shear stress and non-dimensional velocity, temperature and concentration fields as well. We took non-dimensional parametric values as $\kappa_f = 10$, $\varphi = M = Sc = \gamma = 0.1$, $\Pr = 7$, $Rd = 0.5$, $\lambda = 0.2$ for numerical computations. These values were common in the entire study, figures and tables. $f(\eta)$ and $f'(\eta)$ represent tangential and normal velocities while $\theta(\eta)$, $\chi(\eta)$ correspond to temperature and concentration fields, respectively.

For the sake of validity of our computational procedure, we equate our numerical outcomes for $f'(\eta)$, for the limiting case $(M = 0, \phi = 0, Rd = 0, q_r = 0)$, with the ones presented by Asia et al. [30]. An excellent comparison, as seen in Figure 2, confirms the correctness of our computational procedure.

Moreover, special effects of different parameters are described in Figures 3–12 on dimensionless velocities, concentration and temperature curves of nano-fluid flow. The impacts of all dimensionless physical parameters are scrutinized in the figures and tables. Figures 3–5 illustrate the changes in the radius of curvature on tangential velocity $f(\eta)$, normal velocity $f'(\eta)$ and the concentration field $\chi(\eta)$. Both the velocity profiles and concentration field enhance with an increase in the dimensionless radius of curvature. Figures 6–8 portray the effects of the magnetic interaction parameter M on velocities and concentration profiles such that tangential and normal velocities depreciate while the concentration field enhances as we increase the magnetic parameter, which ensures that the fluid's velocity reduces because of the magnetic interaction parameter. In this way, it acts against the radius of the curvature. The variation in the temperature distribution against the change in Prandtl number Pr is depicted in Figure 9. The fluid's temperature was reduced as we increased the Prandtl number. It has also been noticed here that the effect of the Prandtl number is responsible for a decrease in the thermal boundary layer. By keeping other parameters fixed, Figure 10 demonstrates the change in temperature with the radiation parameter, which shows that the temperature profile increases as the values of Rd are increased. Figures 11 and 12 indicate the variation in concentration distribution for Schmidt parameter Sc and chemical reaction parameter γ. It was found that the concentration of the fluid decreased as Sc and γ increased.

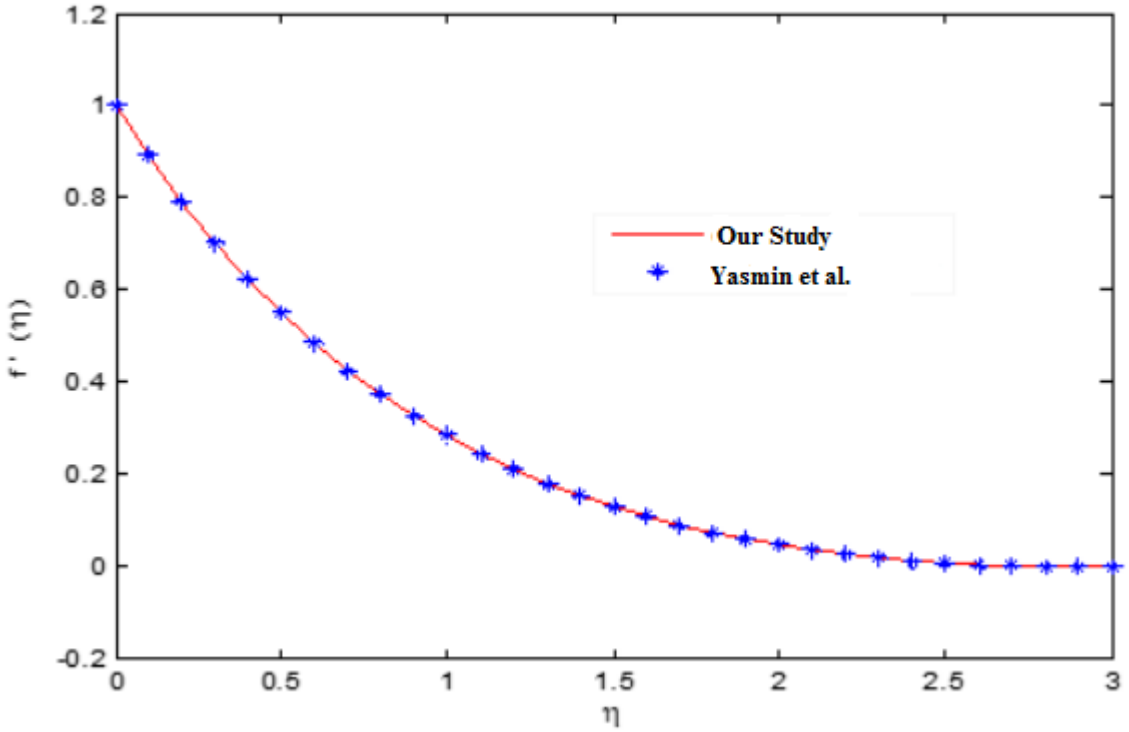

Figure 2. Comparison of the present work by Yasmin et al. [44].

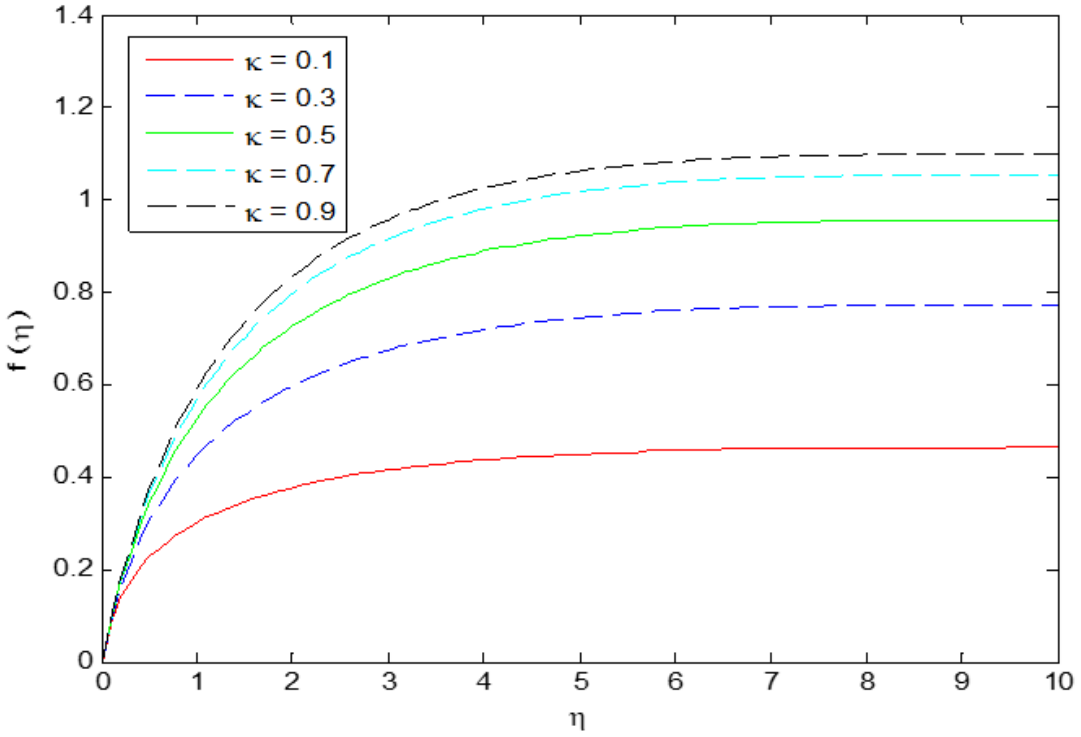

Figure 3. $f(\eta)$ for $M = 0.1$, $\mathrm{Pr} = 7$, $\phi = 0.1$, $Rd = 0.5$, $Sc = 0.1$, $\gamma = 0.1$, $\lambda_1 = 0.2$ and different κ_f.

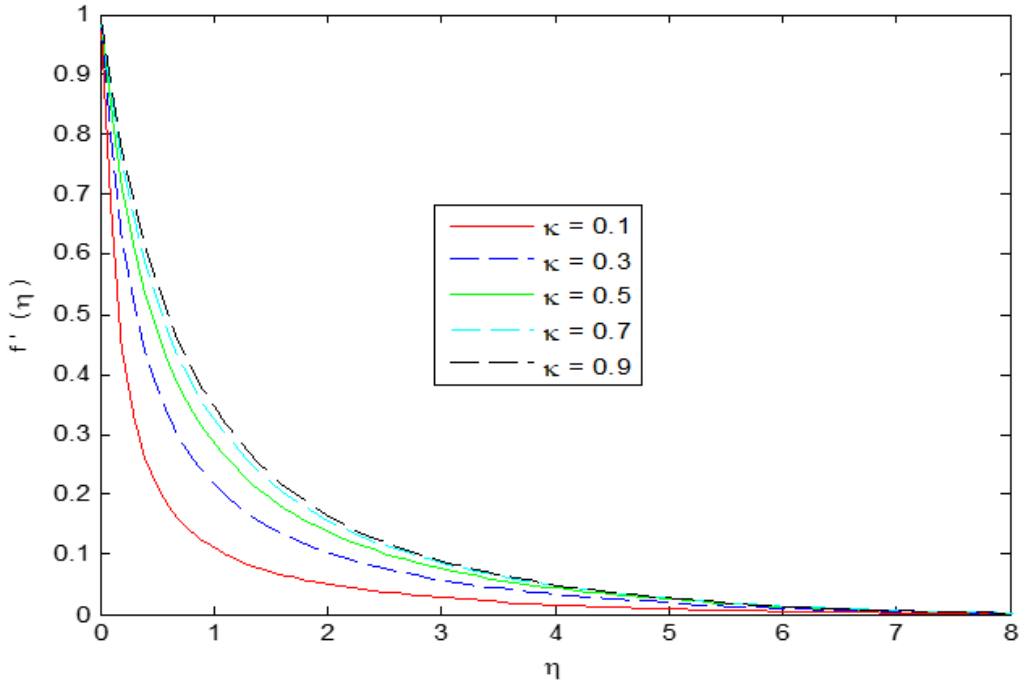

Figure 4. $f'(\eta)$ for $M = 0.1$, Pr $= 7$, $\phi = 0.1$, $Rd = 0.5$, $Sc = 0.1$, $\gamma = 0.1$, $\lambda_1 = 0.2$ and different κ_f.

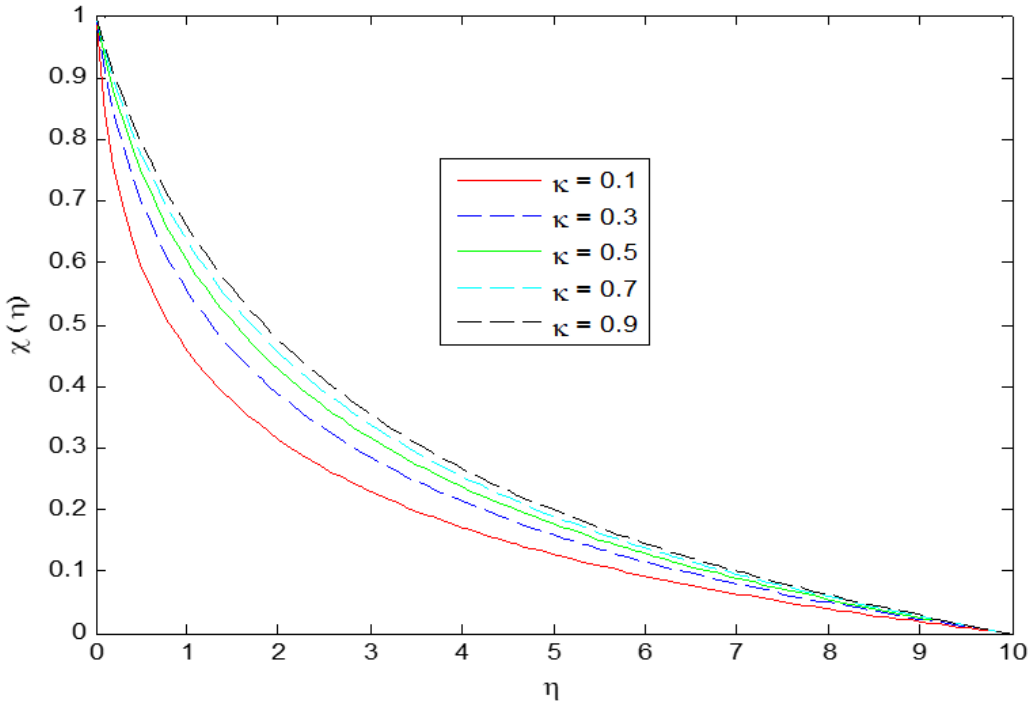

Figure 5. $\chi(\eta)$ for $M = 0.1$, Pr $= 7$, $\phi = 0.1$, $Rd = 0.5$, $Sc = 0.1$, $\gamma = 0.1$, $\lambda_1 = 0.2$ and different κ_f.

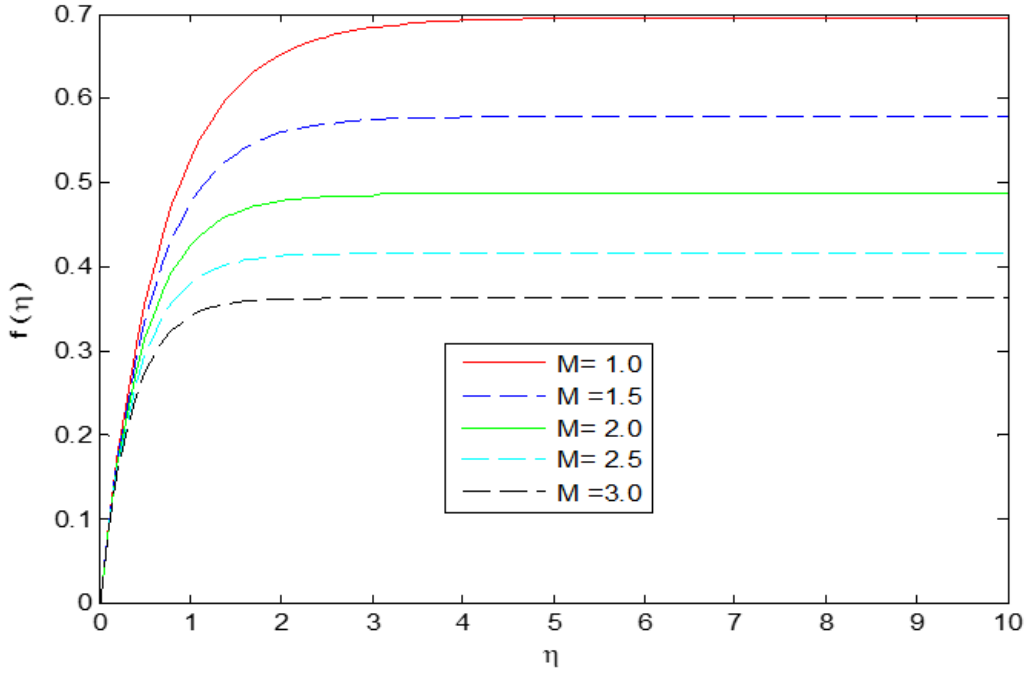

Figure 6. $f(\eta)$ for $k_f = 10,\ \mathrm{Pr} = 7, \phi = 0.1, Rd = 0.5, Sc = 0.1, \gamma = 0.1, \lambda_1 = 0.2$.

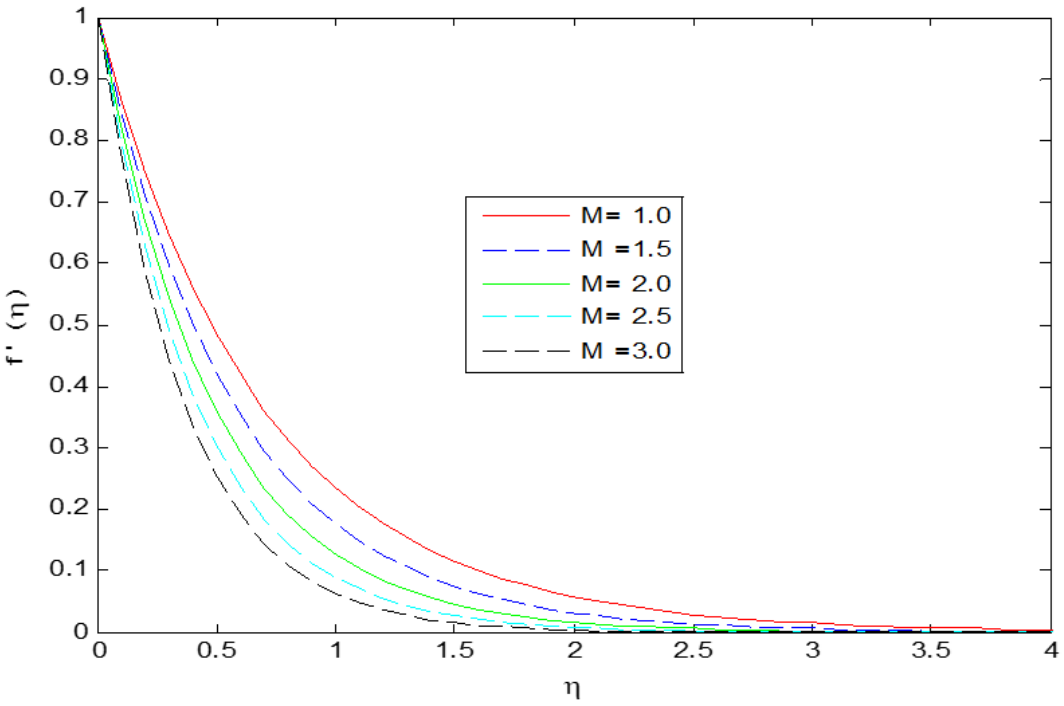

Figure 7. $f'(\eta)$ for $k_f = 10,\ \mathrm{Pr} = 7, \phi = 0.1, Rd = 0.5, Sc = 0.1, \gamma = 0.1, \lambda_1 = 0.2$.

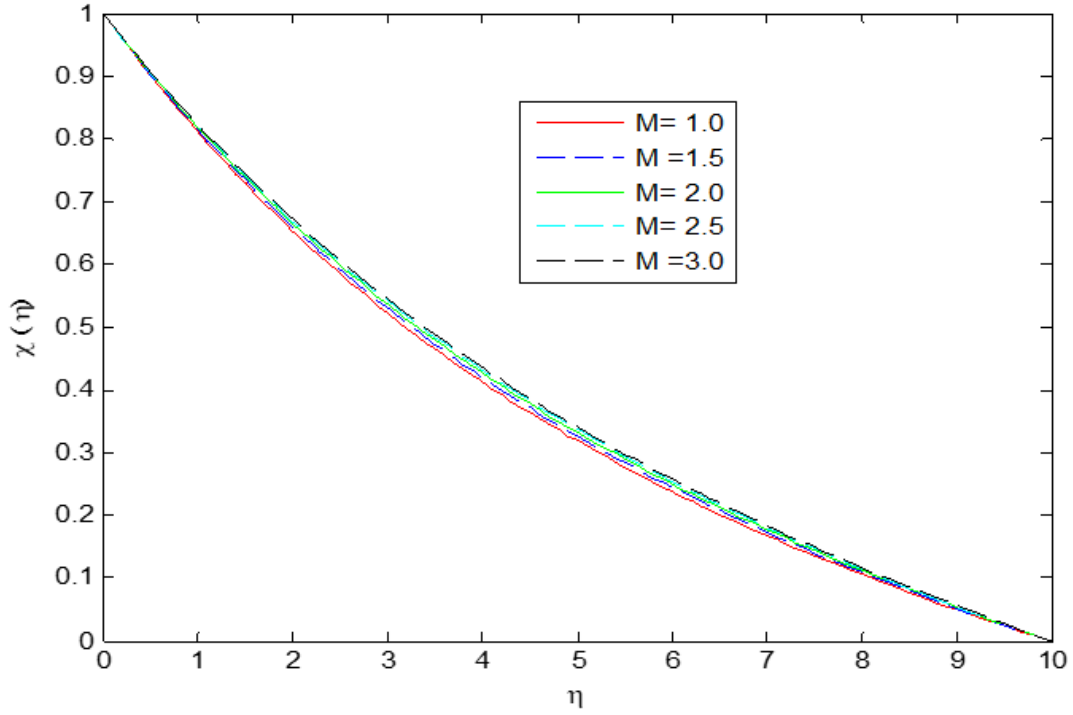

Figure 8. $\chi(\eta)$ for $k_f = 10,\ \mathrm{Pr} = 7, \phi = 0.1, Rd = 0.5, Sc = 0.1, \gamma = 0.1,\ \lambda_1 = 0.2.$

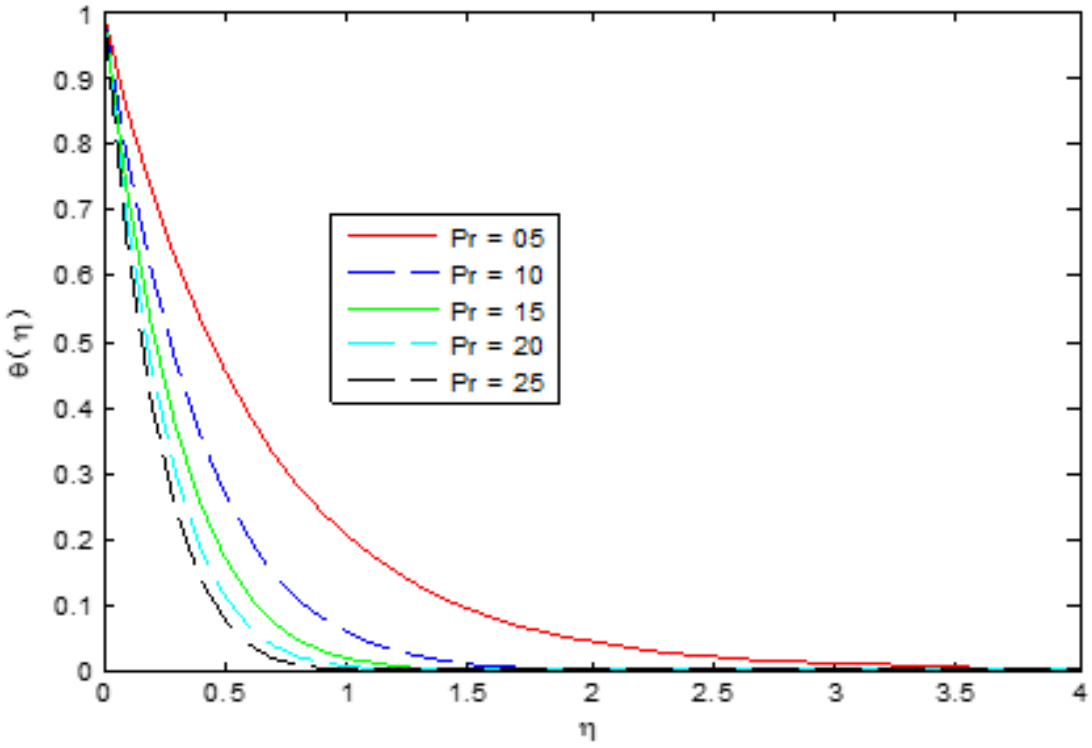

Figure 9. $\theta(\eta)$ for $k_f = 10, M = 0.1, \phi = 0.1, Rd = 0.5, Sc = 0.1, \gamma = 0.1,\ \lambda_1 = 0.2.$

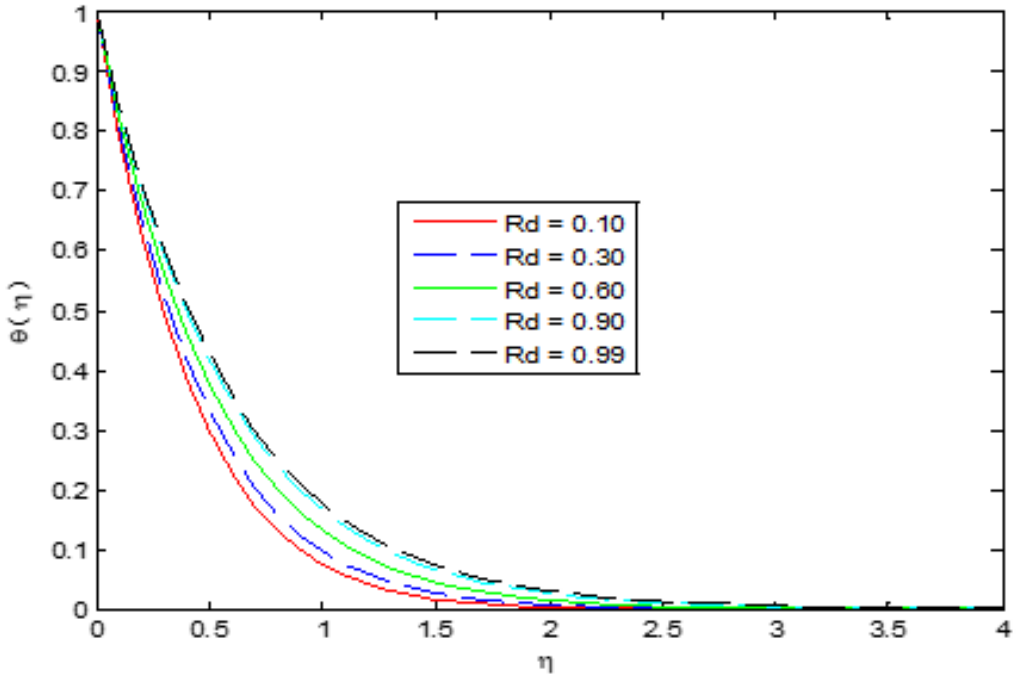

Figure 10. $\theta(\eta)$ for $k_f = 10$, $M = 0.1$, $\phi = 0.1$, Pr $= 7$, $Sc = 0.1$, $\gamma = 0.1$, $\lambda_1 = 0.2$.

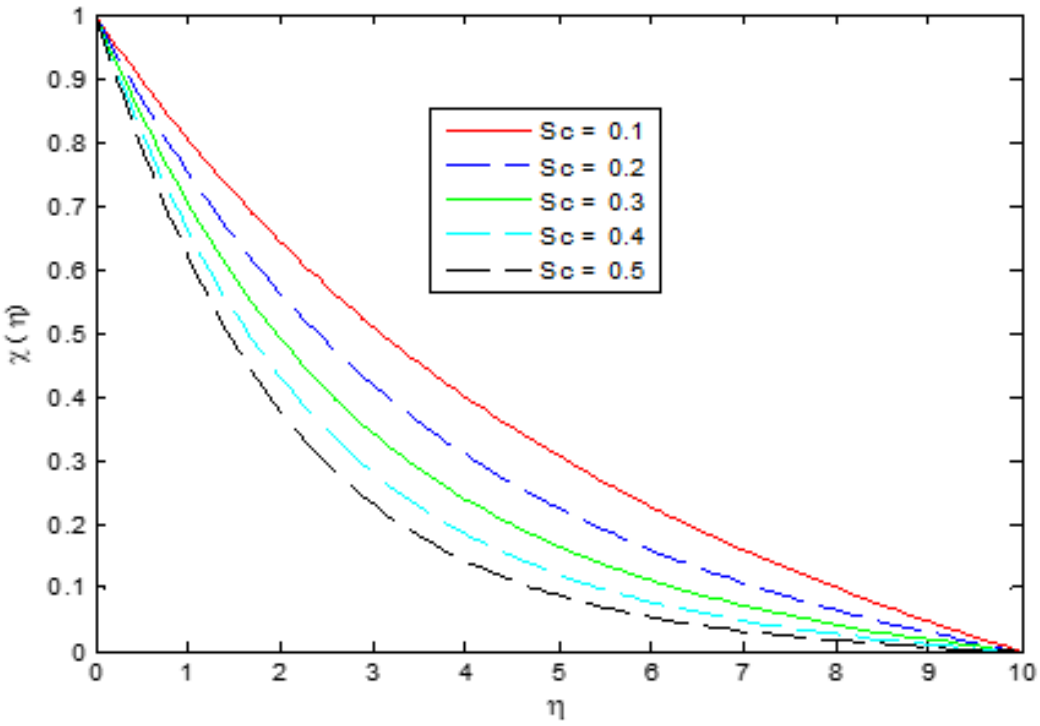

Figure 11. $\chi(\eta)$ for $k_f = 10$, $M = 0.1$, $\phi = 0.1$, Pr $= 7$, $Rd = 0.5$, $\gamma = 0.1$, $\lambda_1 = 0.2$.

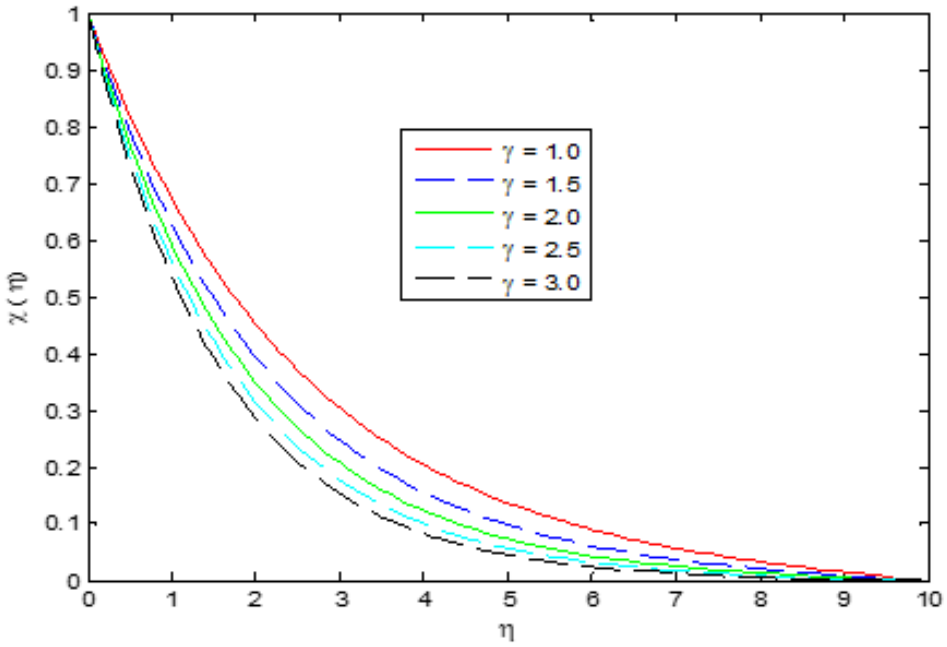

Figure 12. $\chi(\eta)$ for $k_f = 10$, $M = 0.1$, $\phi = 0.1$, Pr $= 7$, $Rd = 0.5$, $Sc = 0.1$, $\lambda_1 = 0.2$.

It is obvious from Table 2 that the dimensionless radius of curvature reduces surface drag, mass and heat transport, while the Hartmann parameter increases shear stress but depreciates the mass and heat transferal rates. Furthermore, in the presence of the Prandtl number, the effect shows that heat transfer is enhanced in Table 3 and depreciates in the presence of the radiation parameter. Table 4 shows that Schmidt parameter and chemical reaction parameter γ elevate the mass transport from the stretching sheet.

Table 2. Numerical values of the radius of curvature and Hartmann number for fixed $\kappa_f = 10$, $M = 0.1$, Pr $= 7$, $Sc = 0.1$, $\phi = 0.1$, $\gamma = 0.1$, $Rd = 0.5$, $\lambda = 0.2$.

κ_f	M	$-f''(0)$	$-\theta'(0)$	$-\chi'(0)$
0.1		9.93356	2.6934	3.280395
0.3		3.88908	1.9148	1.651969
0.5		2.73516	1.8277	1.260395
0.7		2.27919	1.8065	1.077154
0.9		2.04465	1.7993	0.96929
	1	1.67012	1.7318	0.571286
	1.5	1.89177	1.6689	0.570398
	2	2.17357	1.5891	0.569365
	2.5	2.49816	1.4987	0.5683
	3	2.85166	1.4034	0.567278

Table 3. Effect of the Prandlt number and Radiation parameter for fixed $\kappa_f = 10$, $M = 0.1$, $\mathrm{Pr} = 7$, $Sc = 0.1$, $\phi = 0.1$, $\gamma = 0.1$, $Rd = 0.5$, $\lambda = 0.2$.

Pr	***Rd***	$-\theta'(0)$
05		1.461766
10		2.222069
15		2.839614
20		3.359658
25		3.815000
	0.10	2.076521
	0.30	1.916277
	0.60	1.728912
	0.90	1.585597
	0.99	1.548987

Table 4. Effect of the Schmidt number and chemical reaction parameter for fixed $\kappa_f = 10$, $M = 0.1$, $\mathrm{Pr} = 7$, $Sc = 0.1$, $\phi = 0.1$, $\gamma = 0.1$, $Rd = 0.5$, $\lambda = 0.2$.

Sc	γ	$-\chi'(0)$
0.1		0.572105
0.2		0.595779
0.3		0.619490
0.4		0.643226
0.5		0.666975
	0.1	0.629969
	0.3	0.661002
	0.6	0.691290
	0.9	0.720873
	0.99	0.749786

5. Conclusions

In this paper, we presented a comprehensive computational analysis of a viscous nanofluid over a curved extending sheet under the impact of an external magnetic field and thermal radiation. Moreover, we used Newton's difference technique to numerically solve the resultant non-linear equations. Taking distinct values of the involved parameters, we have interpreted the temperature, fluid's velocity and concentration distribution. The consequences are explained with the help of tabular and graphical interpretations. We listed the major consequences of the present work as follows:

- Velocity profiles have shown enhancing behavior for higher values of κ_f while decreasing for magnetic parameter M.
- Temperature profile θ enhances greater values of Rd.
- Skin friction reduces for larger values of chemical reaction parameter γ.
- The Prandtl number tends to reduce the rate of heat transfer.
- The Schmidt number causes an increase in concentration.

The Quasi linearization technique could be applied to a variety of physical and technical challenges in the future [41–52].

Author Contributions: Conceptualization, K.A. and S.A. (Sohail Ahmad); methodology, W.J.; software, K.A.; validation, E.S.M.T.E.D., H.B. and W.J.; formal analysis, W.J.; investigation, S.A. (Shahzad Ahmad); resources, S.A. (Shahzad Ahmad); data curation, W.J.; writing—original draft preparation, S.A. (Sohail Ahmad); writing—review and editing, H.B.; visualization, E.S.M.T.E.D.; supervision, E.S.M.T.E.D.; project administration, E.S.M.T.E.D.; funding acquisition, W.J. All authors have read and agreed to the published version of the manuscript.

Funding: This research received no external funding.

Institutional Review Board Statement: Not applicable.

Informed Consent Statement: Not applicable.

Data Availability Statement: Not applicable.

Conflicts of Interest: The author declares that there is no competing financial and personal relationships interest that can influence the work.

Nomenclature

$l : m$	Cartesian coordinates, [m]
u, v	Velocity components, [ms^{-1}]
c_p	Specific heat, [m^2s^{-2}]
p	Pressure, [$kgm^{-1}s^{-2}$]
k_{nf}	Thermal conductivity of the nano-fluid, [$kgms^{-3}K^{-1}$]
T	Temperature, [K]
Greek Symbols	
μ_{nf}	Dynamic viscosity, [Nsm^{-2}]
ρ_{nf}	Density, [kgm^{-3}]
v_{nf}	Kinematics viscosity, [m^2s^{-1}]
$(\rho c_p)_{nf}$	Heat capacitance of the nano-fluid, [$kgm^{-1}s^{-2}K^{-1}$]

References

1. Naveed, M.; Abbas, Z.; Sajid, M. MHD flow of Micropolar fluid due to a curved stretching sheet with thermal radiation. *J. Appl. Fluid Mech.* **2016**, *9*, 131–138. [CrossRef]
2. Misra, J.C.; Shit, G.C.; Rath, H.J. Flow and heat transfer of a MHD viscoelastic fluid in a channel with stretching walls: Some application to hemodynamic. *J. Sci. Direct* **2008**, *37*, 1–11. [CrossRef]
3. Abass, Z.; Naveed, M.; Sajid, M. Heat transfer analysis for a curved stretching flow over a curved surface with magnetic field. *J. Eng. Thermophys.* **2013**, *22*, 337–345. [CrossRef]
4. Abbas, Z.; Sheikh, M.; Sajid, M. Hydrodynamic stagnation point flow of a micro polar viscoelastic fluid towards a stretching/shrinking sheet in the presence of heat generation. *Can. J. Phys.* **2014**, *92*, 1113–1123. [CrossRef]
5. Hayyat, T.; Abbas, Z.; Javad, T. Mixed convention flow of a micropolar fluid over a non-linear stretching sheet. *Phys. Lett. A* **2008**, *372*, 637–647. [CrossRef]
6. Hayyat, T.; Qasim, M. Effect of thermal radiation on unsteady magnetohydrodynamics flow of micropolar fluid with heat and mass transfer. *J. Nat.* **2010**, *65*, 950–960. [CrossRef]
7. Kanti, P.K.; Sharma, K.V.; Said, Z.; Gupta, M. Experimental investigation on thermo-hydraulic performance of water-based fly ash–Cu hybrid nanofluid flow in a pipe at various inlet fluid temperatures. *Int. Commun. Heat Mass Transf.* **2021**, *124*, 105238. [CrossRef]
8. Kanti, P.; Sharma, K.V.; Ramachandra, C.G.; Gupta, M. Thermal performance of fly ash nanofluids at various inlet fluid temperatures: An experimental study. *Int. Commun. Heat Mass Transf.* **2022**, *119*, 104926. [CrossRef]
9. Bazdar, H.; Toghraie, D.; Pourfattah, F.; Akbari, O.A.; Nguyen, H.M.; Asadi, A. Numerical investigation of turbulent flow and heat transfer of nanofluid inside a wavy microchannel with different wavelengths. *J. Therm. Anal. Calorim.* **2020**, *139*, 2365–2380. [CrossRef]
10. Sarlak, R.; Yousefzadeh, S.; Akbari, O.A.; Toghraie, D.; Sarlak, S.; Assadi, F. The investigation of simultaneous heat transfer of water/$A_{12}O_3$ nanofluid in a close enclosure by applying homogeneous magnetic field. *Int. J. Mech. Sci.* **2017**, *133*, 674–688. [CrossRef]
11. Ishak, A.; Nazar, R.; Pop, I. Heat transfer over a unsteady Stretching permeable surface with prescribe wall temperature, Non-linear analysis. *Nonlinear Anal. Real World Appl.* **2009**, *10*, 2909–2913. [CrossRef]
12. Javad, T.; Ahmad, I.; Abass, Z.; Hayyat, T. Rotating flow of micropolar fluid induced by a stretching Surface. *Z. Für Nat. A* **2010**, *65*, 829–836. [CrossRef]
13. Rasool, G.; Saeed, A.M.; Lare, A.I.; Abderrahmane, A.; Guedri, K.; Vaidya, H. Darcy-Forchheimer Flow of Water Conveying Multi-Walled Carbon Nanoparticles through a Vertical Cleveland Z-Staggered Cavity Subject to Entropy Generation. *Micromachines* **2022**, *13*, 744. [CrossRef] [PubMed]
14. Rasool, G.; Shafiq, A.; Hussain, S.; Zaydan, M.; Wakif, A.; Chamkha, A.J.; Bhutta, M.S. Significance of Rosseland's Radiative Process on Reactive Maxwell Nanofluid Flows over an Isothermally Heated Stretching Sheet in the Presence of Darcy-Forchheimer and Lorentz Forces: Towards a New Perspective on Buongiorno's Model. *Micromachines* **2022**, *13*, 368. [CrossRef] [PubMed]
15. Kumar, L. Finite element analysis of combined heat and mass transfer in hydro magnetic micro polar flow along a stretching sheet. *Comput. Mater. Sci.* **2009**, *46*, 841–848. [CrossRef]
16. Mahmood, M.A.A.; Waheed, S.E. MHD flow and heat transfer of a micropolar fluid over a stretching surface with heat generation (absorption) and slip velocity. *J. Egypt. Math. Soc.* **2012**, *20*, 20–27. [CrossRef]

17. Makinde, O.D. Similarity solution of hydromagnetic heat and mass transfer over a vertical plate with a convective surface boundary condition. *Int. J. Phys. Sci.* **2010**, *5*, 20–27.
18. Nazar, R.; Amin, N.; Filip, D.; Pop, I. Stagnation point flow of a micropolar fluid towards a stretching sheet. *Int. J. Non-linear Mech.* **2004**, *39*, 1227–1235. [CrossRef]
19. Sajid, M.; Ali, N.; Javed, T.; Abbas, Z. Stretching a curved surface in a various fluids. *Chin. Phys. Lett.* **2010**, *27*, 024703. [CrossRef]
20. Sajid, M.; Ali, N.; Javed, T.; Abbas, Z. Flow of a micropolar fluid over a curved stretching surface. *J. Eng. Phys.* **2011**, *84*, 864–871. [CrossRef]
21. Raju, C.S.K.; Sandeep, N.; Sugunamma, V.; JayachandraBabu, M.; Reddy, J.V.R. Heat and mass transfer in magneto-hydrodynamic casson fluid over an exponentially permeable stretching surface. *Eng. Sci. Technol. Int. J.* **2016**, *19*, 45–52.
22. Reddy, P.B. Magneto-hydrodynamic Flow of a Casson Fluid over an Exponentially Inclined Permeable Stretching Surface with Thermal Radiation and Chemical Reaction. *Ain Shams Eng. J.* **2016**, *7*, 593–602. [CrossRef]
23. Ibrahim, S.M.; Lorenzini, G.; Kumar, P.V.; Raju, C.S.K. Influence of chemical reaction and heat source on dissipative MHD mixed convection flow of a Casson nanofluid over a nonlinear permeable stretching sheet. *Int. J. Heat Mass Transf.* **2017**, *111*, 346–355. [CrossRef]
24. Ghadikolaei, S.S.; Hosseinzadeh, K.; Yassari, M.; Sadeghi, H.; Ganji, D.D. Boundary layer analysis of micropolar dusty fluid with TiO_2 nanoparticles in a porous medium under the effect of magnetic field and thermal radiation over a stretching sheet. *J. Mol. Liq.* **2017**, *244*, 374–389. [CrossRef]
25. Khan, I.; Malik, M.Y.; Salahuddin, T.; Khan, M.; Rehman, K.U. Homogenous–heterogeneous reactions in MHD flow of Powell–Eyring fluid over a stretching sheet with Newtonian heating. *Neural Comput. Appl.* **2018**, *30*, 3581–3588. [CrossRef] [PubMed]
26. Nasir, S.; Islam, S.; Gul, T.; Shah, Z.; Khan, M.A.; Khan, W.; Khan, A.Z.; Khan, S. Three-dimensional rotating flow of MHD single wall carbon nanotubes over a stretching sheet in presence of thermal radiation. *Appl. Nanosci.* **2018**, *8*, 1361–1378. [CrossRef]
27. Khan, N.S.; Islam, S.; Gul, T.; Khan, I.; Khan, W.; Ali, L. Thin film flow of a second grade fluid in a porous medium past a stretching sheet with heat transfer. *Alex. Eng. J.* **2018**, *57*, 1019–1031. [CrossRef]
28. Khan, S.A.; Nie, Y.; Ali, B. Multiple slip effects on magnetohydrodynamic axisymmetric buoyant nanofluid flow above a stretching sheet with radiation and chemical reaction. *Symmetry* **2019**, *11*, 1171. [CrossRef]
29. Mabood, F.; Imtiaz, M.; Hayat, T. Features of Cattaneo-Christov heat flux model for Stagnation point flow of a Jeffrey fluid impinging over a stretching sheet: A numerical study. *Heat Transf.* **2020**, *49*, 2706–2716. [CrossRef]
30. Akbar, M.Z.; Ashraf, M.; Iqbal, M.F.; Ali, K. Heat and mass transfer analysis of unsteady MHD nano-fluid flow through a channel with moving porous walls and medium. *AIP Adv.* **2016**, *6*, 045222. [CrossRef]
31. Hady, F.; Ibrahim, F.; El-Hawery, H.; Abdelhady, A. Effects of suction/injection on natural convection boundary layer flow of a nano-fluid past a vertical porous plate through a porous medium. *J. Mod. Methods Numer. Math.* **2012**, *3*, 53–63. [CrossRef]
32. Ahmad, S.; Ali, K.; Saleem, R.; Bashir, H. Thermal Analysis of nano-fluid flow due to rotating cone/plate—A numerical study. *AIP Adv.* **2020**, *10*, 075024. [CrossRef]
33. Iqbal, M.F.; Ahmad, S.; Ali, K.; Akbar, M.Z.; Ashraf, M. Analysis of heat and mass transfer in unsteady nanofluid flow between moving disks with chemical reaction—A Numerical Study. *Heat Transf. Res.* **2018**, *49*, 1403–1418. [CrossRef]
34. Kanti, P.K.; Sharma, K.V.; Minea, A.A.; Kesti, V. Experimental and computational determination of heat transfer, entropy generation and pressure drop under turbulent flow in a tube with fly ash-Cu hybrid nanofluid. *Int. J. Therm. Sci.* **2021**, *167*, 107016. [CrossRef]
35. Kanti, P.; Sharma, K.V.; Said, Z.; Bellos, E. Numerical study on the thermo-hydraulic performance analysis of fly ash nanofluid. *J. Therm. Anal. Calorim.* **2022**, *147*, 2101–2113. [CrossRef]
36. Ruhani, B.; Barnoon, P.; Toghraie, D. Statistical investigation for developing a new model for rheological behavior of Silica–ethylene glycol/Water hybrid Newtonian nanofluid using experimental data. *Phys. A Stat. Mech. Its Appl.* **2019**, *525*, 616–627. [CrossRef]
37. Mashayekhi, R.; Khodabandeh, E.; Akbari, O.A.; Toghraie, D.; Bahiraei, M.; Gholami, M. CFD analysis of thermal and hydrodynamic characteristics of hybrid nanofluid in a new designed sinusoidal double-layered microchannel heat sink. *J. Therm. Anal. Calorim.* **2018**, *134*, 2305–2315. [CrossRef]
38. Arasteh, H.; Mashayekhi, R.; Goodarzi, M.; Motaharpour, S.H.; Dahari, M.; Toghraie, D. Heat and fluid flow analysis of metal foam embedded in a double-layered sinusoidal heat sink under local thermal non-equilibrium condition using nanofluid. *J. Therm. Anal. Calorim.* **2019**, *138*, 1461–1476. [CrossRef]
39. Zari, I.; Shafiq, A.; Rasool, G.; Sindhu, T.N.; Khan, T.S. Double-stratified Marangoni boundary layer flow of Casson nanoliquid: Probable error application. *J. Therm. Anal. Calorim.* **2022**, *147*, 6913–6929. [CrossRef]
40. Shafiq, A.; Mebarek-Oudina, F.; Sindhu, T.N.; Rasool, G. Sensitivity analysis for Walters-B nanoliquid flow over a radiative Riga surface by RSM. *Sci. Iran.* **2022**, *29*, 1236–1249.
41. Batool, S.; Rasool, G.; Alshammari, N.; Khan, I.; Kaneez, H.; Hamadneh, N. Numerical analysis of heat and mass transfer in micropolar nanofluids flow through lid driven cavity: Finite volume approach. *Case Stud. Therm. Eng.* **2022**, *37*, 102233. [CrossRef]
42. Rasool, G.; Shafiq, A.; Khan, I.; Baleanu, D.; Sooppy Nisar, K.; Shahzadi, G. Entropy Generation and Consequences of MHD in Darcy–Forchheimer Nanofluid Flow Bounded by Non-Linearly Stretching Surface. *Symmetry* **2020**, *12*, 652. [CrossRef]

43. Rasool, G.; Shafiq, A.; Alqarni, M.S.; Wakif, A.; Khan, I.; Bhutta, M.S. Numerical Scrutinization of Darcy-Forchheimer Relation in Convective Magnetohydrodynamic Nanofluid Flow Bounded by Nonlinear Stretching Surface in the Perspective of Heat and Mass Transfer. *Micromachines* **2021**, *12*, 374. [CrossRef]
44. Yasmin, A.; Ali, K.; Ashraf, M. Study of heat and mass transfer in MHD flow of micropolar fluid over a curved stretching sheet. *Sci. Rep.* **2020**, *10*, 4581. [CrossRef]
45. Jamshed, W.; Aziz, A. Entropy Analysis of TiO_2-Cu/EG Casson Hybrid Nanofluid via Cattaneo-Christov Heat Flux Model. *Appl. Nanosci.* **2018**, *8*, 1–14.
46. Jamshed, W.; Nisar, K.S. Computational single phase comparative study of Williamson nanofluid in parabolic trough solar collector via Keller box method. *Int. J. Energy Res.* **2021**, *45*, 10696–10718. [CrossRef]
47. Jamshed, W.; Devi, S.U.; Nisar, K.S. Single phase-based study of Ag-Cu/EO Williamson hybrid nanofluid flow over a stretching surface with shape factor. *Phys. Scr.* **2021**, *96*, 065202. [CrossRef]
48. Jamshed, W.; Nisar, K.S.; Ibrahim, R.W.; Shahzad, F.; Eid, M.R. Thermal expansion optimization in solar aircraft using tangent hyperbolic hybrid nanofluid: A solar thermal application. *J. Mater. Res. Technol.* **2021**, *14*, 985–1006. [CrossRef]
49. Jamshed, W.; Nisar, K.S.; Ibrahim, R.W.; Mukhtar, T.; Vijayakumar, V.; Ahmad, F. Computational frame work of Cattaneo-Christov heat flux effects on Engine Oil based Williamson hybrid nanofluids: A thermal case study. *Case Stud. Therm. Eng.* **2021**, *26*, 101179. [CrossRef]
50. Hussain, S.M.; Goud, B.S.; Madheshwaran, P.; Jamshed, W.; Pasha, A.A.; Safdar, R.; Arshad, M.; Ibrahim, R.W.; Ahmad, M.K. Effectiveness of Nonuniform Heat Generation (Sink) and Thermal Characterization of a Carreau Fluid Flowing across a Nonlinear Elongating Cylinder: A Numerical Study. *ACS Omega* **2022**, *7*, 25309–25320. [CrossRef] [PubMed]
51. Pasha, A.A.; Islam, N.; Jamshed, W.; Alam, M.I.; Jameel, A.G.A.; Juhany, K.A.; Alsulami, R. Statistical analysis of viscous hybridized nanofluid flowing via Galerkin finite element technique. *Int. Commun. Heat Mass Transf.* **2022**, *137*, 106244. [CrossRef]
52. Hussain, S.M.; Jamshed, W.; Pasha, A.A.; Adil, M.; Akram, M. Galerkin finite element solution for electromagnetic radiative impact on viscid Williamson two-phase nanofluid flow via extendable surface. *Int. Commun. Heat Mass Transf.* **2022**, *137*, 106243. [CrossRef]